# Geochronology of Galápagos seamounts

Christopher W. Sinton, David M. Christie, and Robert A. Duncan

College of Oceanic and Atmospheric Sciences Oregon State University, Corvallis

**Abstract.** Lavas from seamounts of the central Galápagos Platform and the Carnegie Ridge increase in age with distance from the western edge of the platform, consistent with a hotspot model for the generation of these features. The areal distribution of seamount ages suggests that the pattern of dispersed volcanism seen on the present islands also prevailed between 5 and 6 Ma. Age-distance relationships are consistent with a decrease in the velocity of the Nazca plate relative to the Galápagos hotspot during the past 9 m.y., most likely at ~5 Ma when there was a change in Pacific-hotspot motion. Alternatively, the plate velocity remained constant and volcanism at a single seamount endured up to 7 m.y. Lavas from seamounts along the Wolf-Darwin lineament to the northwest of the Galápagos Platform are young (<1 Ma), with the youngest measured ages closest to the platform.

## Introduction

The Galápagos Archipelago, located just south of the Galápagos Spreading Center (GSC) in the eastern Pacific Ocean (Figure 1), is the present volcanic expression of the Galápagos hotspot. Active volcanism is concentrated on, though not restricted to, the western Galápagos Platform islands of Fernandina and Isabela. The clustering of epicenters of recent earthquakes indicates the present position of the hotspot beneath Isla Fernandina, the largest and most active volcano on the platform. High $^3$He/$^4$He in some Fernandina lavas also implies proximity to the hotspot [*Kurz et al.*, 1993; *Graham et al.*, 1993]. However, unlike a "simple" hotspot, such as Hawaii, where active volcanism occurs in a relatively restricted area, the Galápagos hotspot displays a dispersed and widespread pattern of volcanism; at least nine widely distributed volcanoes have been historically active (Figure 1) [*White et al.*, 1993]. East of Fernandina, there are five active volcanoes on Isla Isabela, and farther east, lavas have erupted within the last century on Isla Santiago and within the last few thousand years on Islas Floreana and Santa Cruz [*White et al.*, 1993]. The easternmost island, San Cristobal, displays a ~3 m.y. span of intermittent volcanism [*Geist et al.*, 1985; *White et al.*, 1993]. Despite the dispersed pattern of volcanism displayed by the islands, the age of earliest volcanic activity increases toward the east, consistent with Nazca plate motion over a fixed mantle plume [*Cox and Dalrymple*, 1966; *Bailey*, 1976; *White et al.*, 1993].

To the north of the larger, central islands is a group of smaller islands (Figure 1). Both Isla Pinta and Isla Marchena have erupted within the last century and the youngest lavas on Isla Genovesa are probably only a few thousand years old [*White et al.*, 1993]. Wolf and Darwin Islands, ~150 km north of Isabela, are part of a NW trending group of seamounts and islands termed the Wolf-Darwin lineament. K-Ar ages of lavas from Wolf and Darwin islands are 0.9-1.6 Ma and 0.4 Ma, respectively [*White et al.*, 1993].

In addition to the emergent volcanoes, there are numerous seamounts within the Galápagos region. In this paper, we present results of K-Ar and $^{40}$Ar-$^{39}$Ar dating of dredged lavas from seamounts and submarine escarpments of the Galápagos Platform and western Carnegie Ridge. At 5-6 Ma, lavas erupted over a region at least 140 km east-west, suggesting that the present broad distribution of active volcanism has persisted for at least 6 m.y. Seamounts of the central Galápagos platform and western Carnegie Ridge increase in age eastward from the western edge of the platform, consistent with a hotspot model for their formation. Age-distance relationships of islands and seamounts on the central platform indicate either a decrease in Nazca plate velocity relative to the hotspot or an increase in the duration of volcanism at a single seamount. Seamounts of the Wolf-Darwin lineament are young (<1 Ma), with the youngest measured ages closest to the platform.

## Sample Description

Samples used in this study were obtained during Leg 2 of the PLUME (PL) expedition of the R/V *Thomas Washington* (Figure 1). Table 1 presents the sample locations, dredge depths, and brief petrological descriptions. Dredge sites on the Carnegie Ridge (PL1) and the eastern Galápagos Platform (PL4-PL8 and PL17) are all seamounts. The samples from these sites are moderately altered basalts notably lacking pillow rim glass. They are predominantly aphyric with some plagioclase-phyric lavas (PL4). Dredge site PL2 is on an escarpment that, based on geographic position and bathymetry, appears to be normal oceanic crust generated at the GSC. Basalts from an escarpment southwest of Isabela (PL22, PL23, and PL24) are very fresh, plagioclase-olivine-phyric basalts with glassy rims. Dredge PL20 recovered variably altered, rounded, basalt pebbles from a small seamount to the east of these dredge sites.

Five dredges from the Wolf-Darwin lineament (PL26 to PL30) recovered very fresh, aphyric and plagioclase-ultraphyric tholeiitic basalts with glassy pillow rims. Sites PL26, PL27, and PL28 are on a large, elongate, composite seamount at the SE end of the Wolf-Darwin lineament and
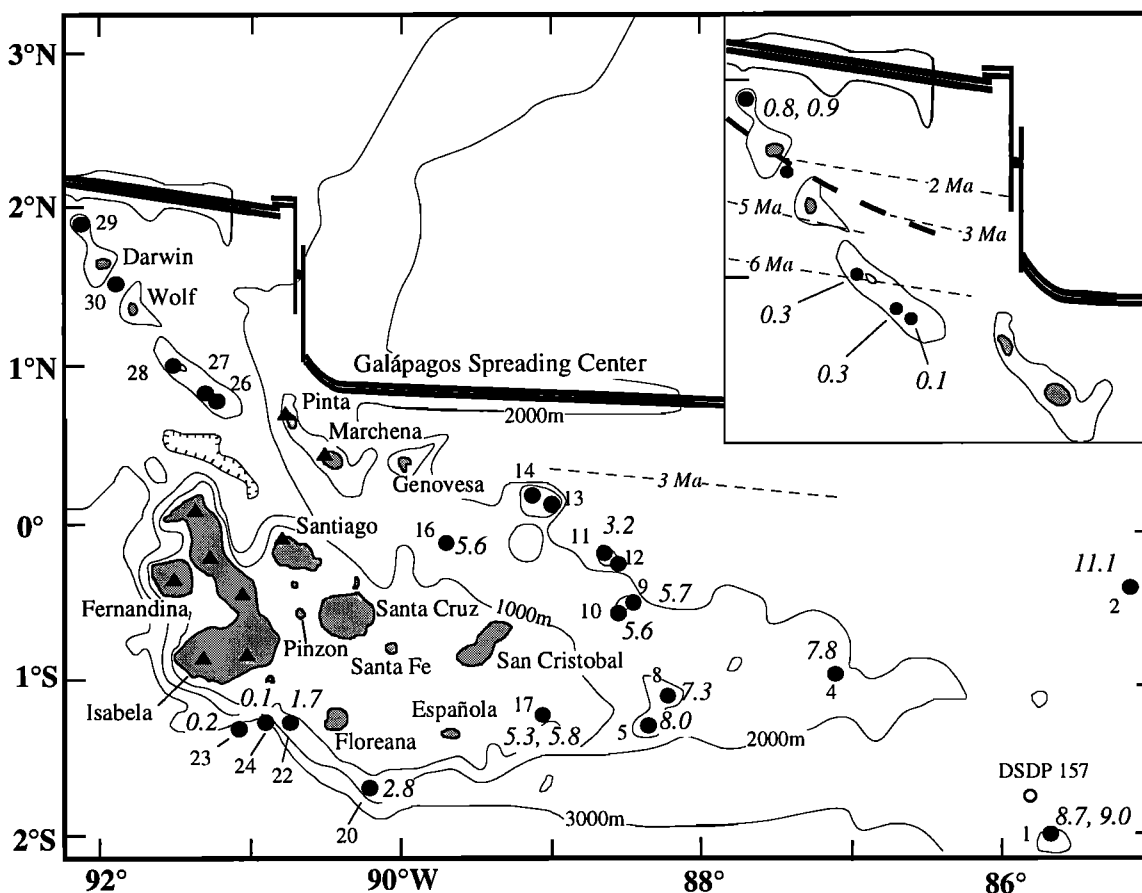
**Figure 1.** The Galápagos Archipelago showing PLUME2 dredge sites (solid circles) and DSDP Site 157 (open circle). Dredge site numbers are labeled and radiometric ages are in italics. Active emergent volcanoes are represented by solid triangles. The inset is a magnification of the Wolf-Darwin lineament. The light dashed lines are approximate positions of magnetic anomaly isochrons, and the heavy dashed line is a pseudofault trace from the westward propagation of the Galápagos Spreading Center (GSC) [*Wilson and Hey*, 1995]. The pseudofault juxtaposes oceanic crust with ~1.8 m.y. difference in age. Bathymetry and location of the GSC are based on work by *Wilson and Hey* (1995) and our unpublished SeaBeam data.

sites PL29 and PL30 are on small, conical seamounts located towards the NW end of the Wolf-Darwin lineament near Wolf and Darwin Islands (Figure 1).

Tholeiitic pillow basalts from three seamounts off the northeastern edge of the platform (PL9-PL14) range from slightly to moderately altered with both glassy and glass-free pillow rims. Rounded cobbles from sites PL11 and PL13 indicate that these seamounts were at one time subaerial [*Christie et al.*, 1992]. Lavas from the northeastern seamounts are rather primitive, and most have MgO > 8% in glass and relatively low $K_2O$ abundances (<0.10% [*Sinton*, 1992]). Most are aphyric, though several plagioclase-ultraphyric or olivine-spinel-phyric lavas were recovered. Two plagioclase-phyric basalts and an olivine-plagioclase-phyric basalt were recovered from dredge site PL16, which was located on a small seamount southeast of Genovesa.

## Analytical Methods

Where possible, we took samples of the freshest and best crystallized material, as far from the pillow rim as possible and from the least altered portion of the rock. However, some

of the older rocks (sites PL1-PL8) were moderately altered throughout. For a suite of rocks from the same dredge, we generally selected the most differentiated samples (highest $K_2O$ contents to assure measurable radiogenic $^{40}Ar$). The $K_2O$ contents of the site PL13 lavas were too low $K_2O$ (0-0.06 %) for radiometric dating.

We used both conventional K-Ar and $^{40}Ar$-$^{39}Ar$ incremental heating methods. One problem associated with dating submarine basalts is that low-temperature alteration in seawater may cause K addition or radiogenic $^{40}Ar$ loss from the sample, resulting in measured ages that are significantly less than the crystallization ages. In this respect, $^{40}Ar$-$^{39}Ar$ incremental heating experiments are considered to be more reliable in dating altered submarine rocks [e.g., *Duncan and Hargraves*, 1990]. The lower-temperature steps release Ar from grain boundaries and other low-retention sites in the rock (fine-grained matrix and alteration phases, such as clays and zeolites) while higher-temperature steps release Ar from unaltered crystal interiors, giving Ar isotopic compositions that more closely reflect the crystallization age. With these criteria in mind, we analyzed the fresh lavas from the southern escarpment by K-Ar. All other samples were analyzed by $^{40}Ar$-$^{39}Ar$, and some were analyzed by both methods.

**Table 1.** Sample Locations and Descriptions

| Sample | Location[†] | Description | Depth[*] (m) |
|---|---|---|---|
| PL1-12 | 02° 01.47'S 85° 40.34'W | seamount; aphyric; vesicular | 2570-2137 |
| PL1-46 | 02° 01.47'S 85° 40.34'W | seamount; aphyric; vesicular | 2570-2137 |
| PL2-02 | 00° 22.40'S 85° 09.70'W | escarpment; aphyric; slightly vesicular | 2610-2140 |
| PL4-19 | 00° 55.92'S 7° 07.46'W | seamount; large plagioclase phenocrysts; slightly vesicular | 1882-1250 |
| PL5-01 | 01° 17.40'S 88° 21.20'W | seamount; aphyric; vesicular | 875-570 |
| PL8-01 | 01° 17.40'S 88° 21.20'W | seamount; aphyric; highly vesicular | 1004-917 |
| PL9-50 | 00° 28.13'S 88° 32.11'W | seamount; plagioclase and olivine microglomerocrysts; vesicular | 1425-935 |
| PL10-05 | 00° 34.04'S 88° 35 44'W | seamount; aphyric; vesicular | 1141-1006 |
| PL11-2 | 00° 11.70'S 88° 40.10'W | seamount; aphyric; vesicular | 1309-702 |
| PL12-1 | 00° 14.45'S 88° 38.20'W | seamount; sparse plagioclase and olivine microphenocrysts; vesicular | 1378-1123 |
| PL14-1 | 00° 06.00'N 89° 05.80'W | seamount; sparse plagioclase and olivine phenocrysts; non-vesicular | 1639-1090 |
| PL16-02 | 00° 06.44'S 89° 49.26'W | seamount; plagioclase and olivine microphenocrysts; non-vesicular | 1688-1320 |
| PL17-01 | 01° 11.38'S 89° 06.58'W | seamount; plagioclase-phyric; non-vesicular | 640-294 |
| PL17-04 | 01° 11.38'S 89° 06.58'W | seamount; aphyric; highly vesicular | 640-294 |
| PL20-02 | 01° 37.73'S 90° 10.70'W | seamount; aphyric; slightly vesicular | 965-310 |
| PL22-01 | 01° 18.23'S 90° 44.92'W | escarpment; sparse plagioclase and olivine phenocrysts; non-vesicular | 1842-1245 |
| PL23-01 | 01° 20.03'S 90° 59.84'W | escarpment; sparse plagioclase and olivine phenocrysts; non-vesicular | 3397-3356 |
| PL24-01 | 01° 18.60'S 90° 55.60'W | escarpment; plagioclase and olivine phenocrysts; slightly vesicular | 3039-2399 |
| PL26-25 | 00° 50.50'N 91° 17.30'W | seamount; sparse plagioclase microphenocrysts; vesicular | 851-500 |
| PL27-17 | 00° 53.80'N 91° 19.80'W | seamount; aphyric; vesicular | 1650-1464 |
| PL28-10 | 01° 00.19'N 91° 33.34'W | seamount; plagioclase-phyric; vesicular | 1454-911 |
| PL29-02 | 01° 54.50'N 92° 10.70'W | seamount; aphyric; slightly vesicular | 1863-1582 |
| PL29-48 | 01° 54.50'N 92° 10.70'W | seamount; aphyric; slightly vesicular | 1863-1582 |
| PL30-01 | 01° 33.63'N 91° 55.66'W | seamount; non-vesicular; sparse plagioclase and olivine microphenocrysts in glassy matrix | 2395-2116 |

[†]Position on-bottom.
[*]On-bottom to off-bottom depths.

Most K-Ar and $^{40}$Ar-$^{39}$Ar samples were crushed in bulk in a ceramic jaw crusher and sieved to a uniform 0.5-1 mm grain size. The exceptions are the $^{40}$Ar-$^{39}$Ar analyses of PL26-PL30 rocks, for which we used 100 mg minicores. All samples were ultrasonically cleaned in distilled water. For the K-Ar analyses, an aliquot of sample was powdered and analyzed for $K_2O$ by atomic absorption spectrophotometry and about 5 g of granular material was fused and the released gas was measured by argon isotopic dilution [*Dalrymple and Lanphere*, 1969]. For the $^{40}$Ar-$^{39}$Ar analyses, 0.5-1.0 g of each granular sample and the mini-cores were sealed in an evacuated quartz glass vial and irradiated for 6 hours at the Oregon State University TRIGA nuclear reactor facility. We monitored neutron flux during irradiation using the Mmhb-1 hornblende (520.4 Ma [*Samson and Alexander*, 1987]) and FCT-3 biotite (27.7 Ma [*Hurfurd and Hammerschmidt*, 1985]) standards.

For both the K-Ar and $^{40}$Ar-$^{39}$Ar experiments (except the minicores), Ar extraction was done in a conventional glass extraction system after the system was baked out at 180°C for at least 12 hours. Samples were heated in outgassed Mo crucibles by radio frequency induction. K-Ar samples were completely fused in one step and the $^{40}$Ar-$^{39}$Ar incremental heating samples were heated in progressively higher temperature steps until fusion. Ideally, each $^{40}$Ar-$^{39}$Ar sample should have as many heating steps as possible without jeopardizing the precision of each step. Because of the low $K_2O$ and relatively young age of the samples, they were analyzed in four or five heating steps. Ar compositions were then measured using an Associated Electrical Industries (AEI) MS-10S mass spectrometer.

Each minicore was heated in a temperature-controlled resistance furnace. In order to minimize atmospheric contamination, the samples were preheated to 450°C and the released gas was pumped away. Then the samples were heated in five sequential 150°C steps from 600° to 1400°C (fusion). Ar from the minicore samples was measured using a low-blank Mass Analyzer Products (MAP) 215-50 mass spectrometer.

K-Ar ages were calculated using the methods described by

**Table 2.** Results from K-Ar and $^{40}Ar$-$^{39}Ar$ Radiometric Dating

| Sample | K-Ar Age* $\pm 1\sigma$ (Ma) | Plateau Age* $\pm 1\sigma$ (Ma) | % $^{39}Ar$ | Isochron $\pm 1\sigma$ (Ma) | N† | SUMS/ (N-2) | $^{40}Ar/^{36}Ar_i$ § $\pm 1\sigma$ | Distance (km) |
|---|---|---|---|---|---|---|---|---|
| PL1-12 | 5.78 ± 0.43 | 8.7 ± 0.4 | 100 | 8.1 ± 0.5 | 4 | 0.63 | 297.0 ± 1.9 | 624 |
| PL1-46 | 5.07 ± 0.22 | 9.1 ± 0.4 | 100 | 9.0 ± 0.1 | 4 | 0.05 | 295.7 ± 1.2 | 624 |
| PL2-02 | 0.89 ± 0.07 | 11.1 ± 1.4 | 80.5 | 10.2 ± 1.6 | 3 | 0.17 | 298.6 ± 13.3 | -- |
| PL4-19 | -- | 7.8 ± 1.2 | 100 | 10.4 ± 5.5 | 4 | 0.50 | 292.3 ± 2.0 | 453 |
| PL5-01 | -- | 8.0 ± 1.5 | 100 | 8.0 ± 8.3 | 5 | 6.30 | 287.2 ± 4.2 | 314 |
| PL8-01 | -- | 7.3 ± 0.5 | 100 | 7.0 ± 0.3 | 4 | 0.02 | 296.2 ± 7.3 | 330 |
| PL9-50 | -- | 5.7 ± 0.6 | 86.2 | 4.2 ± 2.1 | 3 | 0.74 | 301.0 ± 9.8 | 295 |
| PL10-5 | 1.10 ± 0.11 | 5.6 ± 1.4 | 82.8 | 6.0 ± 0.4 | 3 | 0.01 | 293.9 ± 8.8 | 295 |
| PL11-2 | -- | 3.2 ± 0.5 | 100 | 3.2 ± 0.3 | 5 | 0.88 | 296.6 ± 2.9 | 280 |
| PL12-1 | 0.63 ± 0.11 | -- | -- | -- | -- | -- | -- | -- |
| PL14-1 | 8.95 ± 1.65 | -- | -- | -- | -- | -- | -- | -- |
| PL16-2 | -- | 5.6 ± 0.3 | 93.8 | 5.2 ± 0.1 | 4 | 0.05 | 302.6 ± 6.2 | 165 |
| PL17-1 | -- | 5.3 ± 0.4 | 95.2 | 5.1 ± 0.3 | 4 | 0.51 | 298.0 ± 7.0 | 235 |
| PL17-4 | -- | 5.8 ± 0.8 | 100 | 5.5 ± 0.6 | 5 | 0.63 | 298.0 ± 7.0 | 235 |
| PL20-2 | -- | 2.8 ± 0.3 | 94.3 | 3.1 ± 0.2 | 4 | 0.13 | 291.6 ± 7.6 | 107 |
| PL22-1 | 1.69 ± 0.06 | -- | -- | -- | -- | -- | -- | 43 |
| PL23-1 | 0.18 ± 0.04 | -- | -- | -- | -- | -- | -- | 10 |
| PL24-1 | 0.14 ± 0.02 | -- | -- | -- | -- | -- | -- | 16 |
| PL26-25 | 0.03 ± 0.13 | 0.1 ± 0.1 | 87.7 | -0.1 ± 0.1 | 4 | 2.08 | 299.1 ± 1.9 | -- |
| PL27-17 | 0.13 ± 0.16 | 0.3 ± 0.1 | 68.1 | -0.2 ± 0.1 | 3 | 0.02 | 296.2 ± 3.1 | -- |
| PL28-10 | 0.34 ± 0.17 | 0.3 ± 0.1 | 92.0 | 0.4 ± 0.5 | 4 | 0.94 | 293.3 ± 3.0 | -- |
| PL29-2 | 0.03 ± 0.05 | 0.9 ± 0.1 | 47.9 | 0.7 ± 0.2 | 3 | 0.29 | 293.6 ± 4.4 | -- |
| PL29-48 | 1.60 ± 0.07 | 0.8 ± 0.2 | 66.7 | 1.2 ± 1.4 | 3 | 1.50 | 290.5 ± 4.7 | -- |
| PL30-1 | 0.25 ± 0.05 | 1.7 ± 0.1 | 52.4 | 4.3 ± 1.7 | 3 | 0.82 | 276.0 ± 3.4 | -- |

*Ages are calculated using $\lambda_\varepsilon$= 0.581 x $10^{-10}$ $yr^{-1}$ and $\lambda_\beta$= 4.962 x $10^{-10}$ $yr^{-1}$, K-Ar ages are calculated using $^{40}K/K$=1.167x$10^{-4}$ mol/mol.

†Number of steps used in the plateau and isochron age calculations.

§Initial $^{40}Ar/^{36}Ar$ based on the inverse of the y-intercept of the regression.

*Dalrymple and Lanphere* [1969] after correction for mass fractionation (Table 2). Individual ages for each $^{40}Ar$-$^{39}Ar$ step were calculated using corrections for background, mass fractionation, and isotopic interferences. From the heating steps, age spectrum diagrams (age versus % $^{39}Ar$ released) were generated (Figure 2). We calculated plateau ages from consecutive steps that are concordant within 1σ error using the procedure described in *Dalrymple et al.* [1988], in which step ages were weighted by the inverse of their variance (Table 2). It is possible, however, that the lavas did not completely equilibrate with an atmospheric Ar composition ($^{40}Ar/^{36}Ar$ = 295.5) upon crystallization. We investigated this possibility by plotting isotope correlation diagrams ($^{36}Ar/^{40}Ar$ versus $^{39}Ar/^{40}Ar$) in which the slope is proportional to the age and the inverse of the y-intercept gives the initial $^{40}Ar/^{36}Ar$ composition in the crystallized rock. For each sample, steps from the plateau age were used in the regression. The goodness-of-fit parameter SUMS [*York*, 1969] has a $\chi^2$-distribution with (N-2) degrees of freedom, N being the number of steps included in the isochron regression (Table 2). For example, a value of SUMS/(N-2) = 2.6 for N=5 should only be exceeded for one sample out of 20 based on Gaussian distribution of measurement error; analogous values are 3.0 for N=4 and 3.8 for N=3. Of all the samples, only PL5-1 exceeded the 95% confidence limit.

## Results

For the purposes of discussion, we divide the Galápagos Platform into three regions: the Wolf-Darwin lineament, the northeast seamounts and islands, and the central platform/Carnegie Ridge (Figure 1). The Wolf-Darwin lineament includes Wolf and Darwin Islands and dredge sites PL26-PL30. The northeast volcanoes are the islands of Pinta, Marchena, and Genovesa and the seamount dredge sites PL9-PL14. The rest of the islands and dredge sites (except PL2) are included in the central platform and western Carnegie Ridge (Figure 1). The PL9-PL10 seamount, which could be in either of the latter two regions, is included with the northeast volcanoes because its lavas are similar in composition to the other volcanoes in this group [*Sinton*, 1992].

## The Central Platform/Carnegie Ridge

Samples PL1-12 and PL1-46 gave reliable $^{40}Ar$-$^{39}Ar$ ages of about 9 Ma with statistically indistinguishable plateau and isochron ages and nearly atmospheric initial $^{40}Ar/^{36}Ar$ ratios (Table 2 and Figure 2). The K-Ar ages from the same samples are, however, significantly younger than the $^{40}Ar$-$^{39}Ar$ ages. Judging from the altered condition of the samples (clays filling vesicles and cracks), it is likely that the K-Ar ages reflect loss of radiogenic $^{40}Ar$ and/or addition of secondary $K_2O$ during low-temperature alteration, and therefore the $^{40}Ar$-$^{39}Ar$ ages are the more accurate. Planktonic foraminifera in the sediments overlying the basaltic basement at Deep Sea Drilling Project (DSDP) Site 157 (near site PL1) are of the *Globorotalia plesiotumida* zone [*Kaneps*, 1973], giving a minimum age of 11 to 6 Ma [*Berggren et al.*, 1996]. However, poor preservation in the sediments above the basement suggests that the basaltic crust could be older. This is indicated by magnetic isochrons from *Lonsdale and Klitgord* [1978] which show that the PL1 seamount overlies crust of magnetic chron 5Cn (17 to 16 Ma) [*Berggren et al.*, 1996]. Assuming that the magnetic isochrons accurately represent the age of the oceanic crust, the PL1 lavas are 7 to 8 m.y. younger than the underlying crust.

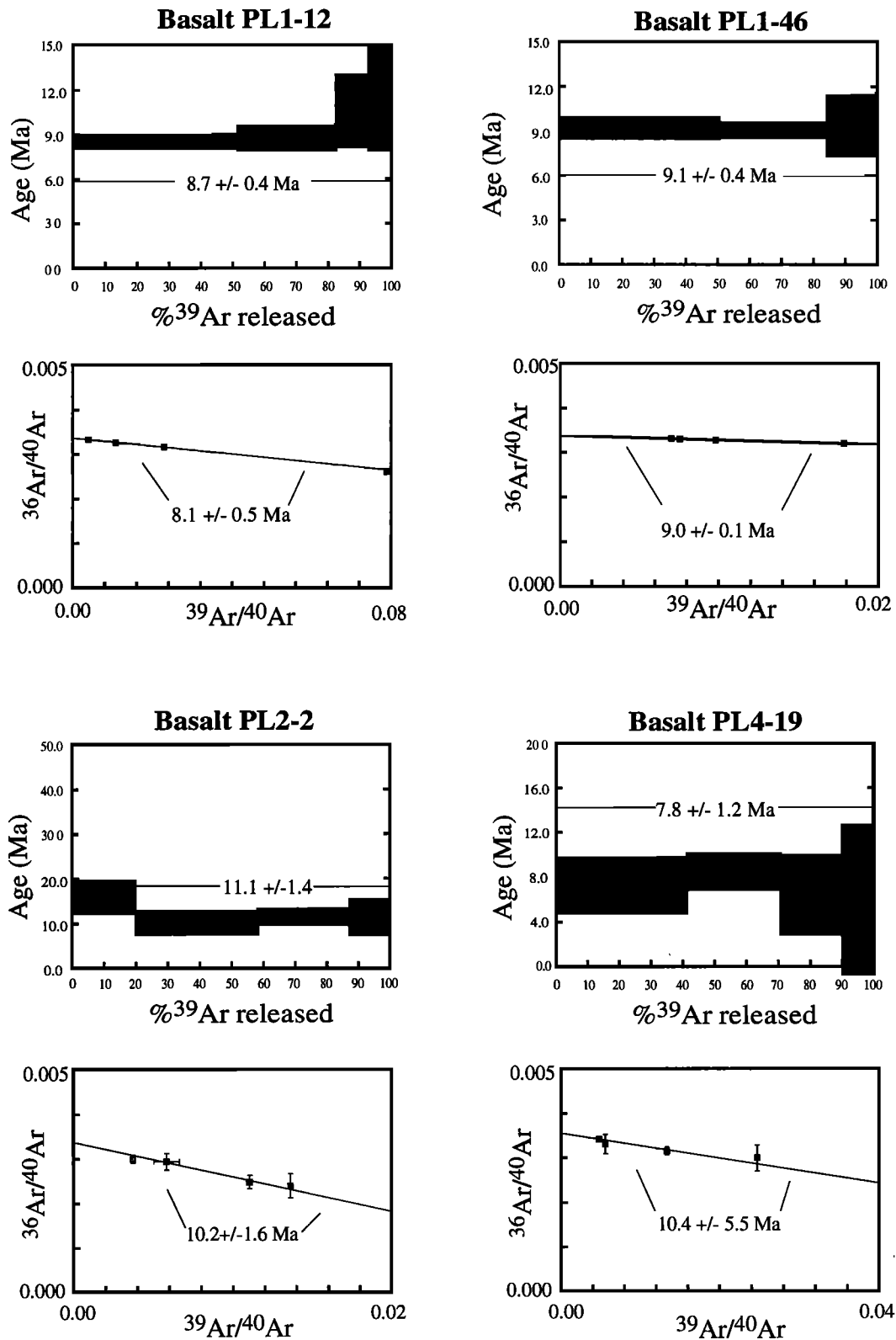Samples from dredge sites on the central platform (PL4,

## Basalt PL1-12



8.7 +/- 0.4 Ma

%$^{39}$Ar released

8.1 +/- 0.5 Ma

$^{39}$Ar/$^{40}$Ar

## Basalt PL1-46



9.1 +/- 0.4 Ma

%$^{39}$Ar released

9.0 +/- 0.1 Ma

$^{39}$Ar/$^{40}$Ar

## Basalt PL2-2



11.1 +/-1.4

%$^{39}$Ar released

10.2+/-1.6 Ma

$^{39}$Ar/$^{40}$Ar

## Basalt PL4-19



7.8 +/- 1.2 Ma

%$^{39}$Ar released

10.4 +/- 5.5 Ma

$^{39}$Ar/$^{40}$Ar

**Figure 2.** Step age spectra and isotope correlation diagrams for each $^{40}$Ar-$^{39}$Ar analysis. The length of each step age refers to the fraction of the total $^{39}$Ar released and the thickness of the step is the ± 1σ error. The light horizontal lines adjacent to the plateau age span the steps used in the age calculation. The solid squares in the correlation diagrams indicate the data points used in a weighted linear regression to obtain an isochron age. Open squares were excluded from the regression. The inverse of the y-intercept of the regression gives the initial $^{40}$Ar/$^{36}$Ar ratio.

## Basalt PL5-1



## Basalt PL8-1
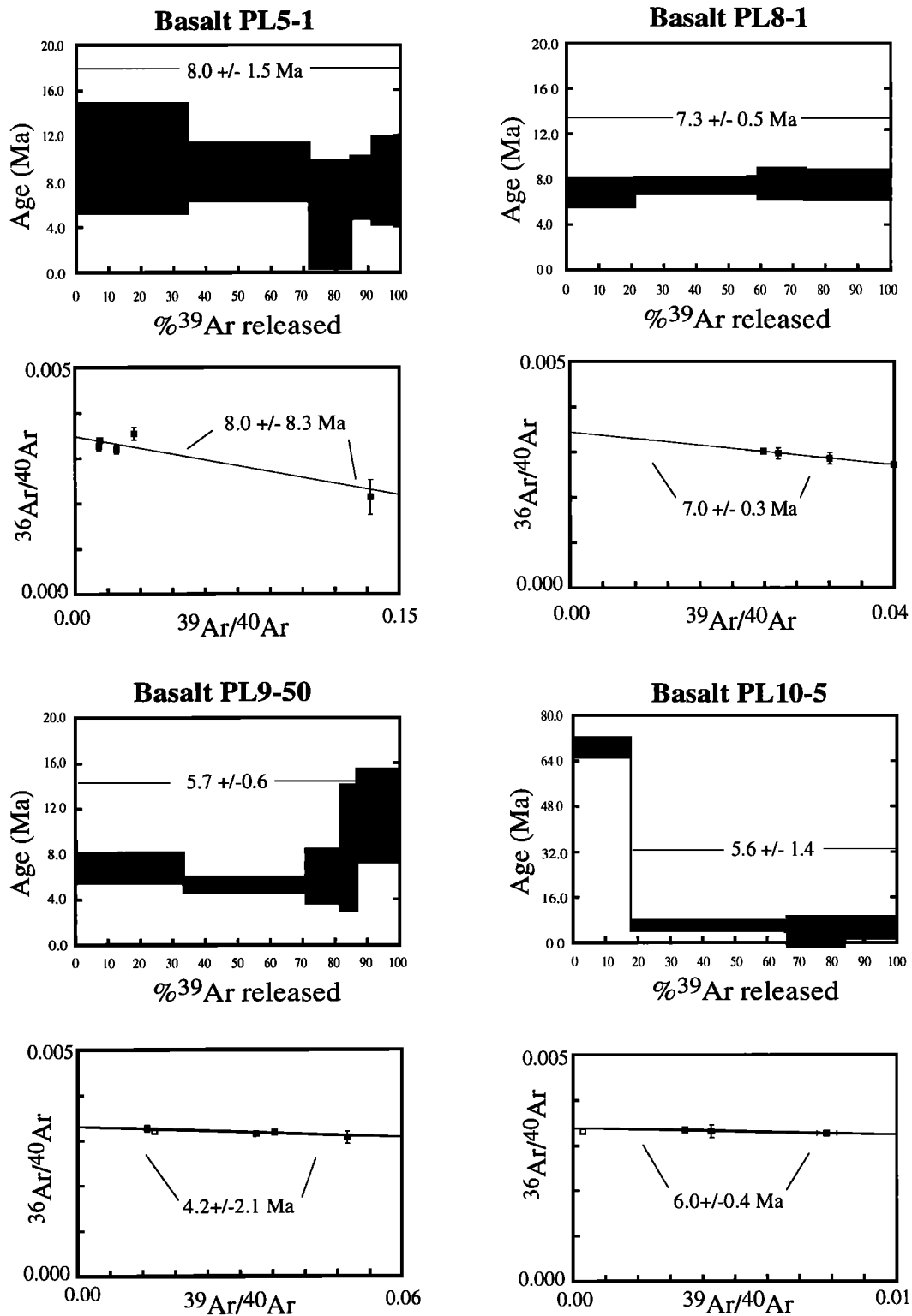


## Basalt PL9-50



## Basalt PL10-5



**Figure 2.**  (continued)

PL5, PL8, PL16, and PL17) yielded reliable $^{40}$Ar-$^{39}$Ar ages, although the isochron ages from PL4-19 and PL5-1 have high uncertainties (Figure 2 and Table 2). Lavas from PL22, PL23, and PL24 were analyzed by K-Ar only. Although there are no internal checks on the reliability of their measured ages, the results are most likely meaningful because of the freshness of the samples, the high $K_2O$ content, and the similarity of the ages to nearby Isabela Island [*White et al.*, 1993].

### Northeast Volcanoes

Because of the low $K_2O$ contents of the northeastern seamount lavas, $^{40}$Ar-$^{39}$Ar experiments were performed on the most differentiated samples from PL9, PL10, PL11, and PL16. K-Ar analyses were also performed on samples from PL10, PL12, and PL14. The K-Ar age from site PL10 is younger than the corresponding $^{40}$Ar-$^{39}$Ar age, so we use the $^{40}$Ar-$^{39}$Ar age
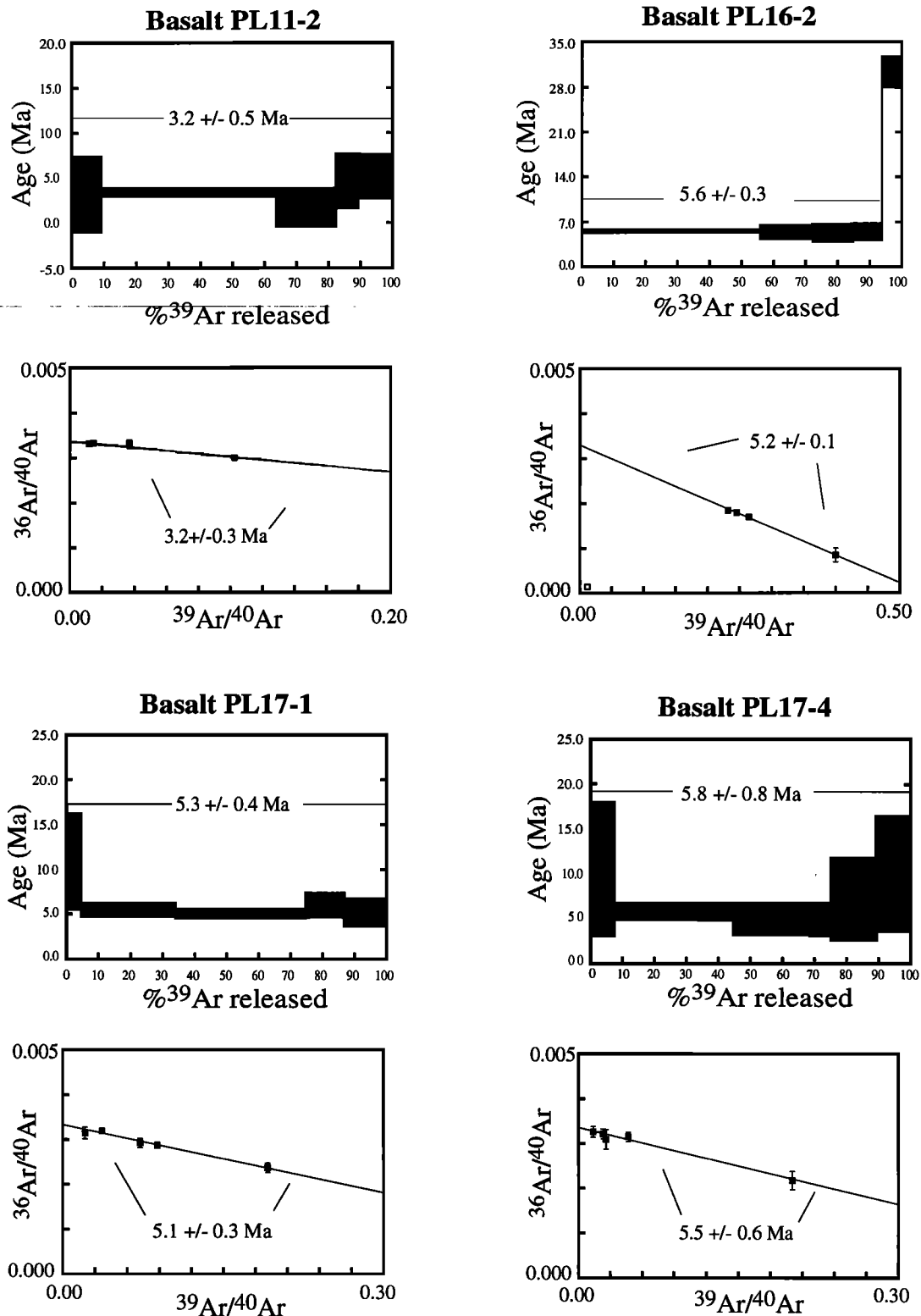
Figure 2. (continued)

as representative of the crystallization age. Based on these results, the PL9-PL10, PL11-PL12, and PL16 seamounts were formed by 5.7 Ma, 3.2 Ma, and 5.6 Ma, respectively (Table 2). PL14-1 gave a K-Ar age of 9.0 Ma, considerably older than the magnetic age of the underlying crust (Figure 1) [*Wilson and Hey*, 1995]. This sample apparently contained excess radiogenic $^{40}$Ar. Because of the low $K_2O$ of this lava, and its necessarily young age, the amount of K-supported radiogenic

Ar is small, and so even a small amount of retained mantle-derived Ar would have a significant effect on the measured age.

## Wolf-Darwin Lineament

The K-Ar ages from sites PL26-PL28 (0.03-0.34 Ma) are within 1σ error of the $^{40}$Ar-$^{39}$Ar ages (0.1-0.3 Ma) (Table 2). However, the two methods give different ages for the site PL29

## Basalt PL20-2



## Basalt PL26-25


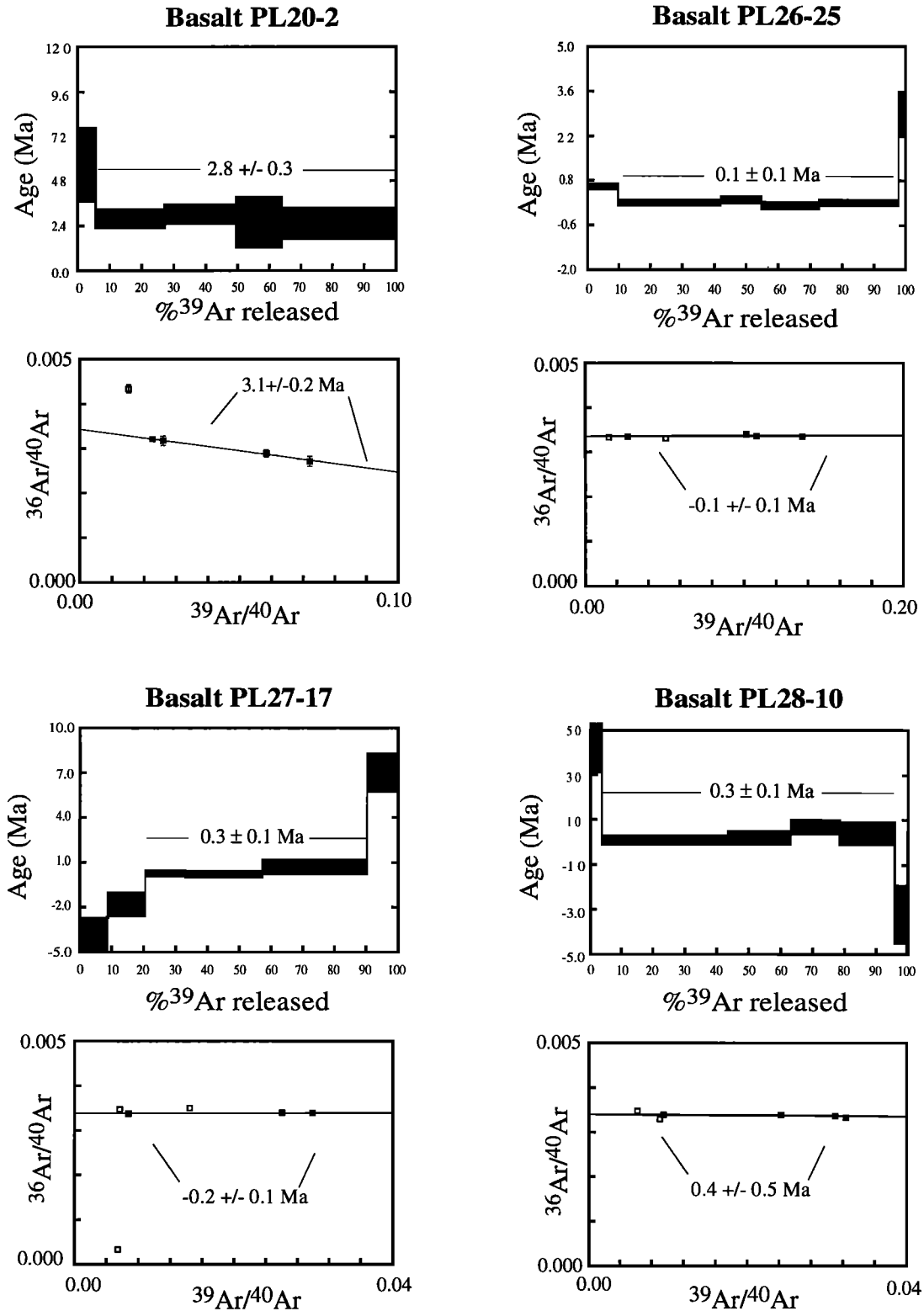
## Basalt PL27-17



## Basalt PL28-10



**Figure 2.** (continued)

and PL30 lavas. Two PL29 lavas yielded K-Ar ages of 0.03 ± 0.05 and 1.60 ± 0.07 Ma. The $^{40}$Ar-$^{39}$Ar age spectra from both these samples are disturbed and show evidence of excess radiogenic $^{40}$Ar in the first and last steps. Despite this, the middle steps for both samples give similar integrated plateau ages (0.9 ± 0.1 Ma and 0.8 ± 0.2 Ma). Isochron ages using the

same steps as the plateaus are concordant with the plateau ages (within analytical uncertainty) and near-atmospheric initial $^{40}$Ar/$^{36}$Ar ratios. Together, the data indicate a crystallization age of 0.8-0.9 Ma for these lavas. The disturbed age spectrum from PL30-1 and the disagreement between the K-Ar age (0.25 ± 0.05 Ma), the integrated age for the first two steps of the
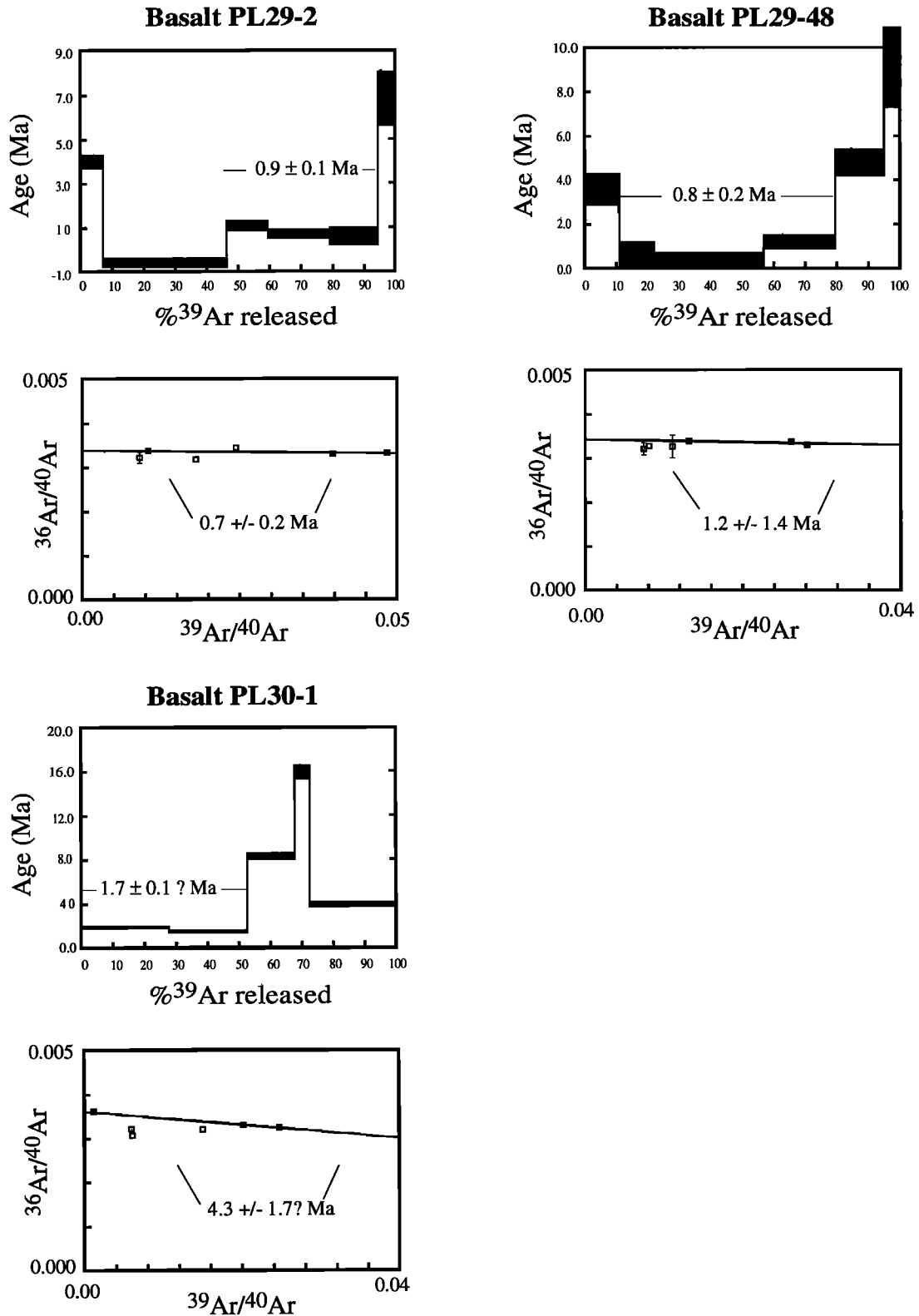
## Basalt PL29-2



## Basalt PL29-48



## Basalt PL30-1



**Figure 2.** (continued)

$^{40}$Ar-$^{39}$Ar spectrum (1.7 ± 0.1 Ma), and the isochron age (4.4 ± 0.5 Ma; from the first three steps) casts doubt on whether any of these ages are meaningful.

### Site PL2

Sample PL2-2 gave a reliable $^{40}$Ar-$^{39}$Ar age with statistically indistinguishable plateau and isochron ages and near-atmospheric initial $^{40}$Ar/$^{36}$Ar ratios (Table 2 and Figure 2). Like the PL1 samples, the K-Ar age is significantly younger than the $^{40}$Ar-$^{39}$Ar age, and therefore we consider the $^{40}$Ar-$^{39}$Ar age to represent the crystallization age. Dredge site PL2 is near a possible pseudofault according to the magnetic isochron map of *Wilson and Hey* [1995]. To the west of the site, the age of the crust is 7-8 Ma (chron 4n) [*Berggren et al.*, 1996], much younger than the 11.1 ± 1.4 Ma age of the PL2

lava. About 70 km to the east, chron 5An (12.5-12.0 Ma) was identified as by *Lonsdale and Klitgord* [1978]. If the PL2 lava is associated with this crustal section, then it must have originated at the Costa Rica rift.

## Discussion

### Past Patterns of Volcanism

By examining the distribution of coeval lavas on the Galápagos Platform, we can assess the past patterns of volcanism and compare these to the present pattern. Lavas from three seamounts from the central platform (sites PL16, PL9-PL10, and PL17) have ages between 5 and 6 Ma (Figure 1). These locations are distributed over an area that is comparable to the present distribution of active volcanism (excluding the Wolf-Darwin lineament). This implies that widespread and dispersed volcanism was a characteristic of the Galápagos hotspot between 5 and 6 Ma, when the spreading center was centered over the hotspot [*Hey et al.*, 1977; *Wilson and Hey*, 1995]. We infer that dispersed volcanism may be a long-term characteristic of the Galápagos hotspot.

### Hotspot-Nazca Plate Velocity

The ages of submarine samples from the central platform and Carnegie Ridge increase toward the east (Figures 1 and 3), extending the general age progression seen in the islands [*Christie et al.*, 1992; *White et al.*, 1993]. These data are consistent with Nazca plate motion over a stationary mantle plume presently located beneath Fernandina volcano and can be used to estimate Nazca plate-hotspot velocities over the past 9 m.y.

Previous estimates of the velocity of the Nazca plate relative to the hotspot have been calculated by adding the hotspot-Pacific motion to the Pacific-Nazca motion. *Minster and Jordan* [1978] calculated a velocity of 49 ± 8 km/m.y. using their Pacific-Nazca velocity from magnetic anomalies averaged over the past 3 m.y. and a hotspot-Pacific velocity from K-Ar ages (<10 Ma) along Pacific island chains. *Gripp and Gordon* [1990] used a different Pacific-Nazca velocity [*DeMets et al.*, 1990] (also averaged over the past 3 m.y.) and the same hotspot-Pacific velocity [*Minster and Jordan*, 1978] to derive a Nazca-hotspot velocity of 37 ± 7 km/m.y., lower but within error of the *Minster and Jordan* [1978] estimate.

The Nazca-hotspot velocity can be directly estimated by plotting the ages of the Galápagos lavas relative to the distance from the hotspot. Because Galápagos volcanism is dispersed, simple backtracking of a sample site in the direction of plate motion will not necessarily arrive at Isla Fernandina. In addition, volcanism can persist at a single island for at least 3 m.y. [*White et al.*, 1993], so lavas can erupt well to the east of their contemporaneous hotspot location. This can be a particular problem with the seamount lavas because there is no stratigraphic information obtained by dredging.

To produce the age versus distance plot of Figure 3, we make the assumption that all sampled lavas were erupted along a line of longitude (91°W) through the east coast of Isla Isabela. The distance from this line to the sample is measured along the azimuth of Nazca plate motion (102°). Figure 3 shows that there has been a broad areal distribution of coeval lavas for at least the past 5-6 m.y. Volcanism has clearly been long-lived at some locations, most notably Isla San Cristobal, which is

the farthest island from the hotspot (180-200 km) and, at 5-6 Ma, seamount lavas have a broad areal distribution. Nevertheless, for the last 6 m.y., maximum age increases linearly eastward from the hotspot; these maximum ages define the hotspot-Nazca plate velocity for the interval 6 to 0 Ma. In calculating this rate, the < 6 Ma dredge ages (PL11, PL16, and PL22-PL24) are combined with the oldest K-Ar ages from each of the central islands (Floreana, 1.52 Ma; Pinzon, 1.4 Ma; and Santa Fe, 2.8 Ma) [*White et al.*, 1993]. A regression weighted to the inverse of the error for each sample is fitted to the data points and the inverse of the slope yields a velocity of 39.2 ± 0.2 km/m.y., within error of the 37± 7 km/m.y. velocity calculated by *Gripp and Gordon* [1990]. Sample PL16 falls well to the left of this line, indicating that it erupted as much as 50 km west of the hotspot.

It is apparent from Figure 3 that the 39 km/m.y. line passes well above some of the older lavas. This can be interpreted as reflecting either a decrease in the Nazca-hotspot velocity at 5-6 Ma or as an artifact of increasingly prolonged volcanism at each site as well as the preferential sampling of younger lavas inherent in dredging. The dark shaded region on Figure 3 is the field of lavas that would have erupted up to 180 km east of the hotspot (the approximate distance of San Cristobal from Isla Isabela) assuming a constant 39 km/m.y. velocity over time. While this region encompasses the data points from most of the submarine lavas, it does not include the site PL1 samples. For this site, a constant plate velocity of 39 km/m.y. would predict an age of 15.9 Ma (the approximate age of the underlying crust) and, consequently, a 7 m.y. span of volcanism. So either the duration of volcanism was much longer at >9 Ma than it is presently or, alternatively, there has been a decrease in the Nazca-hotspot velocity.

A change in the hotspot-Pacific motion at 5 Ma is evident from a change in the Pacific-Juan de Fuca relative motion and the sudden onset of deformation and uplift along the San Andreas fault [*Cox and Engebretson*, 1985, and references therein]. *Cox and Engebretson* [1985] calculated the angular velocity of hotspot-Pacific rotation poles as 0.73°/m.y. (from 19.5 Ma to 5 Ma) and 0.97°/m.y. (5-0 Ma). They suggested that this change in plate motion could be due to the detachment of a subducting slab beneath the New Hebrides arc. Because there was no apparent change in the Pacific-Nazca spreading rate between the Oligocene and the Plio-Pleistocene [*Handschumacher*, 1976], the increase in the WNW movement of the Pacific plate should have resulted in a 32% decrease in the eastward velocity motion of the Nazca plate over the Galápagos hotspot. Assuming a discrete change in plate motion and a constant length-scale of dispersed volcanism (~180 km), we can estimate the Nazca-hotspot plate velocity prior to 5 Ma from Figure 3 by pivoting the envelope at 5 Ma until the shaded area encompasses site PL1. This yields a minimum plate velocity of about 57 km/m.y. (Figure 3). A 32% decrease in this value gives a 5-0 Ma Nazca-hotspot velocity of 39 km/m.y. and agrees with the change in plate motion put forth by *Cox and Engebretson* [1985].

Although the data are consistent with a change in the hotspot-Nazca velocity at ~5 Ma, this conclusion hinges on one critical site and further dating of lavas from the Carnegie Ridge would be needed to test this assertion. The alternative interpretation of the age-distance relations is that the hotspot-Nazca plate velocity has remained constant and Galápagos hotspot volcanism at 16 to 9 Ma was more dispersed than it was 9-0 Ma. For San Cristobal, K-Ar ages range from 2.35 to 0.05 Ma [*White et al.*, 1993], but if we assume that the island
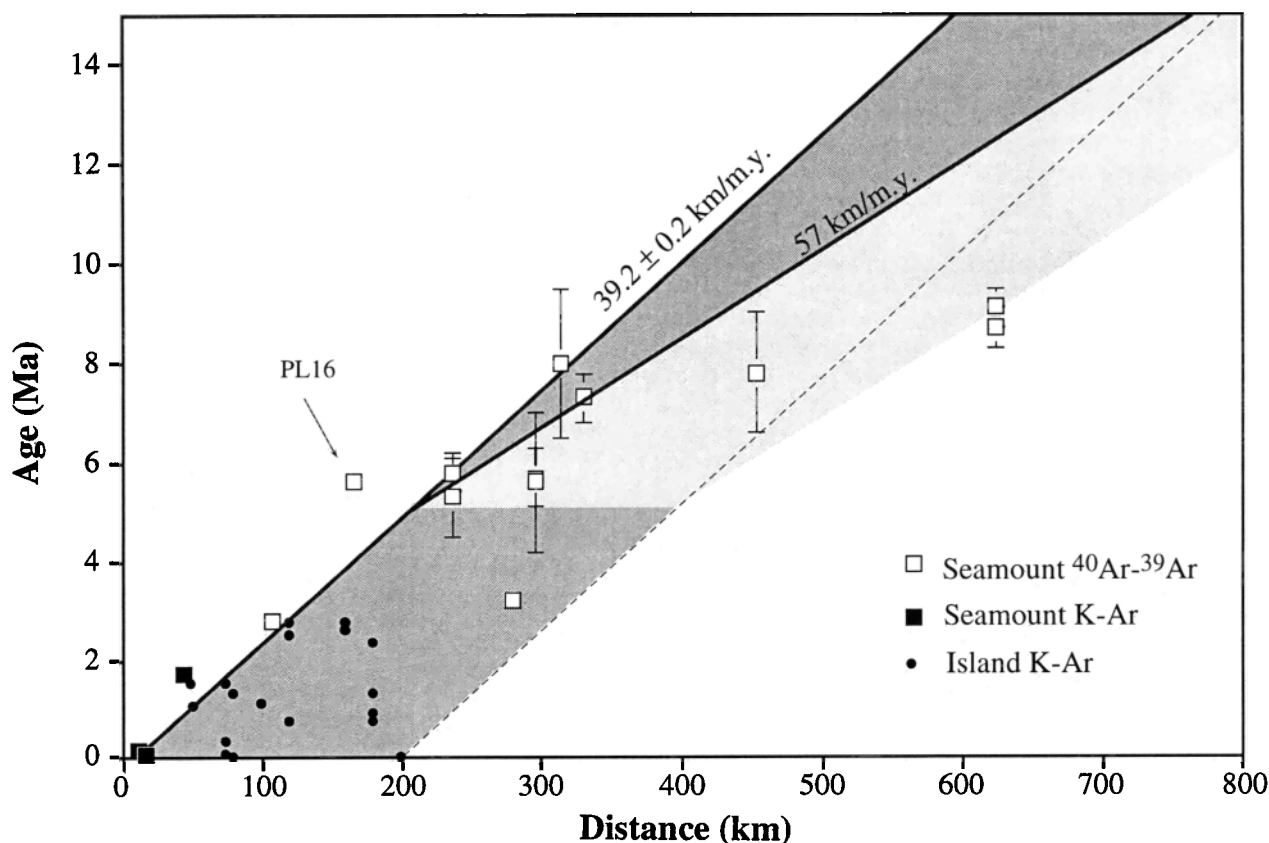
**Figure 3.** Plot of age versus distance from the east coast of Isla Isabela for the dredged lavas and the oldest eastward island lavas. The data set is made of the dredge $^{40}$Ar-$^{39}$Ar ages (open squares) and K-Ar ages (solid squares) and the K-Ar ages from the islands (solid circles [*White et al.*, 1993]). Error bars are 1σ uncertainty. The solid line is a weighted regression fitted to the < 6 Ma dredge ages and the island ages. The darker shaded region is the field of lavas that would have erupted up to 180 km from Isla Isabela assuming a constant velocity of 39 km/m.y. The lighter shaded region represents the possible age range of lavas erupted up to 180 km from Isla Isabela prior to 5 Ma if the plate velocity were ~57 km/m.y.

initially formed directly over the hotspot, volcanism would have spanned almost 5 m.y., shorter than the 7 m.y. span of volcanism implied for site PL1 by a constant plate speed.

A wider dispersion and longer span of hotspot volcanism could presumably have occurred if the Galápagos Spreading Center resided over the hotspot during this interval, as this would provide a channeling mechanism for volcanism away from the plume. According to the plate reconstructions of *Hey* [1977], the hotspot was producing a volcanic trail solely on the Cocos plate from <15 to 10 Ma and not on the Nazca plate. He inferred a lack of hotspot volcanism on the Nazca plate at this time from the "saddle," i.e., the deeper bathymetry, between the Carnegie Ridge and the eastern Galapagos Platform. This argues against wider dispersion of volcanism due to spreading ridge channeling between 16 and 9 Ma at site PL1.

Taken together, the present data are consistent with either a decrease in the hotspot-Nazca plate velocity or an increase in the areal region of hotspot volcanism. At this point, neither of the interpretations is more credible than the other.

**Wolf-Darwin Lineament**

The Wolf-Darwin lineament is a roughly linear array of seamounts and two small islands. A pseudofault of the 93°W/95.5°W propagating rift cuts obliquely through the

lineament at Darwin Island [*Wilson and Hey*, 1995]. The northern part of the Wolf-Darwin lineament encompasses four conical volcanoes, Wolf and Darwin Islands, a small seamount (site PL29; ~10 km diameter, summit depth ~1350 m) NW of Darwin, and a small seamount (site PL30; ~3 km diameter, summit depth ~2000 m) between Wolf and Darwin. The southern part of the lineament is an elongate seamount (sites PL26-PL28; ~70 km long, summit depth ~400 m) that is morphologically distinct from the NW Wolf-Darwin lineament volcanoes and slightly offset in a right-stepping en echelon pattern. Rather than a conical shape, this seamount has a hummocky morphology and appears to be a composite structure, constructed of numerous smaller volcanic cones (unpublished SeaBeam data). The lavas from this seamount (PL27 and PL26) are very young, indicating active or very recent volcanism. This is consistent with epicenters of recent earthquakes in the area [see *Feighner and Richards*, 1994].

The mechanism(s) controlling the location and orientation of the Wolf-Darwin lineament is not clearly understood. *Morgan* [1978] proposed that the volcanoes of the Wolf-Darwin lineament formed at a spreading ridge and that the linear alignment of the volcanoes is a vector sum of northward jumps of the GSC and the absolute motion of the Nazca plate. This model predicts that the seamount ages should increase away from the spreading center and towards the hotspot, from

NW to SE. *Feighner and Richards* [1994] suggested, on the basis of gravity observations, that the Wolf-Darwin lineament overlies a "lithospheric fault", although there is no indication of strike-slip or dip-slip offset. This suggests a model in which volcanism occurs in response to lithospheric tearing that allows mantle upwelling and melting. In this model, volcanism can occur randomly along the lineament.

Our new radiometric ages constrain such models. The PL29 lavas (0.8 and 0.9 Ma), which lie 30-40 km from the ridge crest, could have erupted at the GSC, consistent with either hypothesis. However, the young (probably still active) volcanism at the SE end of the Wolf-Darwin lineament and the K-Ar ages from the Wolf and Darwin Islands ( 0.9-1.6 Ma and 0.4 Ma, respectively) [*White et al.*, 1993] are not consistent with the Morgan (1978) model unless these volcanoes formed at the ridge and continued erupting as they moved from the ridge. If this were the case, then volcanism at the SE end of the Wolf-Darwin lineament must have been continuous since 6 Ma, the approximate age of the crust at this point (Figure 3) [*Wilson and Hey*, 1995]. This seems improbable for such a small edifice. Overall, the lack of a clearly defined age progression along the lineament is most consistent with lithospheric weaknesses controlling the location volcanism.

## Conclusions

We have used radiometric ages of lavas dredged from the Galápagos Platform and western Carnegie Ridge to identify past volcanic patterns as well as constrain the hotspot-Nazca velocity over the past 9 m.y. Widespread volcanism on the Galápagos Platform at 5-6 Ma indicates that the current dispersed pattern of volcanism dates back to at least this time. The ages of the earliest lavas from the central Galápagos Platform and the Carnegie Ridge increase progressively eastward from the western edge of the platform, consistent with a hotspot model for the generation of these features. Age-distance relationships suggest either a decrease in the Nazca-hotspot velocity, most likely at 5 Ma, or a 7-m.y. span of volcanism on the oldest of the sampled seamounts. Rocks dredged from the entire length of the Wolf-Darwin lineament are young (<1 Ma). Although the youngest measured lavas are farthest from the GSC, there is no clear trend along the lineament. The pattern of volcanism along the Wolf-Darwin lineament does not fit the hotspot model; perhaps here volcanism is controlled by the stress pattern around the ridge-transform environment, with thermal and material input from the hotspot.

## References

Bailey, K, Potassium-argon ages from the Galápagos Islands, *Science*, *192*, 465-466, 1976.

Berggren, W. A., D. V. Kent, C. C. Swisher, and M.-P. Aubrey, , A revised Cenezoic geochronology and chronostratigraphy, in *Geochronology, Time Scales and Global Stratigraphic Correlations: A Unified Temporal Framework for an Historical Geology*, edited by W. A. Berggren, D. V Kent,. and J. Hardenbol, Soc. of Econ. Paleontolo. and Mineral., Tulsa, Okla., in press, 1996.

Christie, D.M., R.A. Duncan, A.R. McBirney, M.A. Richards, W.M. White, K.S. Harpp, C.G. and Fox, Drowned islands downstream from the Galápagos hotspot imply extended speciation times, *Nature*, *355*, 246-248, 1992.

Cox, A., and G.B. Dalrymple, Paleomagnetism and potassium-argon ages of some volcanic rocks from the Galápagos Islands, *Nature*, *209*, 776-777, 1966.

Cox, A., D. and Engebretson, Change in motion of Pacific plate at 5 M.y.r BP, *Nature*, *313*, 472-474, 1985.

Dalrymple, G.B., M.A. and Lanphere, *Potassium Argon Dating: Principles, Techniques, and Application to Geochronology*, 258 pp., W.H. Freeman, New York, 1969.

Dalrymple, G. B., D. A. Clague, T. L. Vallier, and H. W. Menard, $^{40}Ar/^{39}Ar$ age, petrology, and tectonic significance of some seamounts in the Gulf of Alaska, in *Seamounts, Islands, and Atolls, Geophys. Monogr.Ser.*, vol. 43, edited by B. H. Keating, P. Fryer, R. Batiza, and G. W. Boehlert, pp. 297-315, AGU, Washington, D.C., 1988.

DeMets, C., R.G. Gordon, D.F. Argus, and S. Stein, Current plate motions, *Geophys. J. Int.*, *101*, 425-478, 1990.

Duncan, R. A., and R.B. Hargraves, $^{40}Ar/^{39}Ar$ geochronology of basement rocks from the Mascarene Plateau, Chagos Bank, and Maldives Ridge, *Proc. Ocean Drilling Program, Sci. Results*, *115*, 43-52, 1990.

Feighner, M.A., and M.A. Richards, Lithospheric structure and compensation mechanisms of the Galápagos Archipelago, *J. Geophys. Res.*, *99*, 6711-6729, 1994.

Geist, D.J., W.M. White, and R.A. Duncan, Geology and petrogenesis of lavas from San Cristobal Island, Galápagos Archipelago, *Geol. Soc. Am. Bull.*, *97*, 555-566, 1985.

Graham, D.W., D.M. Christie, K.S. Harpp, and J.E. Lupton, Mantle plume helium in submarine basalts from the Galápagos Platform, *Science*, *262*, 2023-2026, 1993.

Gripp, A.E., and R.G. Gordon, Current plate velocities relative to hotspots incorporating the NUVEL-1 global plate model, *Geophys. Res. Lett.*, *17*, 1109-1112, 1990.

Handschumacher, D.W., Post-Eocene plate tectonics of the eastern Pacific, in *The Geophysics of the Pacific Ocean Basin, Geophys. Monogr. Ser.*, vol. 19, edited by G. Sutton, M.H. Manghnani, and R. Moberly, pp. 177-202, AGU, Washington, D.C., 1976.

Hey, R., Tectonic evolution of the Cocos-Nazca spreading center, *Geol. Soc. Am. Bull.*, *88*, 1404-1420, 1977.

Hey R., G.L. Johnson, and A. Lowrie, Recent plate motions in the Galápagos area, *Geol. Soc. Am. Bull.*, *88*, 1385-1403, 1977.

Hurfurd, A.J., and K. Hammerschmidt, $^{40}Ar/^{39}Ar$ nd K-Ar dating of the Bishop and Fish Canyon Tuffs: Calibration ages for fission-track dating standards, *Chem. Geol.*, *58*, 23-32, 1985.

Kaneps, A.G., Cenozoic planktonic formaminifers, eastern equatorial Pacific Ocean, *Initial Rep. Deep Sea Drill. Proj.* *16*, 713-745, 1973.

Kurz, M.D., D.P. Kammer, T.C. Kenna, and D. Geist, Dynamics and evolution of the Galápagos hotspot from helium isotopes, *Eos Trans. AGU, 74 (43)*, Fall Meet. Suppl., 632, 1993.

Lonsdale, P., and K.D. Klitgord, Structure and tectonic history of the eastern Panama basin, *Geol. Soc. Am. Bull.*, *89*, 981-999, 1978.

Minster, J.B., and T.H. Jordan, Present-day plate motions, *J. Geophys. Res.*, *83*, 5331-5354, 1978.

Morgan, W.J., Rodriguez, Darwin,.., a second type of hotspot island, *J. Geophys. Res.*, *83*, 5355-5360, 1978.

Samson, S.D., and E.C. Alexander, Jr, Calibration of the inter-laboratory $^{40}Ar/^{39}Ar$ dating standard MMhb-1, *Chem. Geol.*, *66*, 27-34, 1987.

Sinton, C.W., The evolution of the Galápagos Platform: Results from radiometric dating and experimental petrology, M.S. thesis, 117 pp., Oreg. State Univ., Corvallis, 1992.

White, W.M., A.R. McBirney, and R.A. Duncan, Petrology and geochemistry of the Galápagos Islands: Portrait of a pathological mantle plume, *J. Geophys. Res.*, *98*, 19533-19563, 1993.

Wilson, D.S., and R.N. Hey, History of rift propogation and magnetization intensity for the Cocos-Nazca spreading center, *J. Geophys. Res.*, *100*, 10041-10056, 1995.

York, D., Least-squares fitting of a straight line with correlated errors, *Earth Planet. Sci. Lett.*, 5, 320-324, 1969.

D.M. Christie, R.A. Duncan, and C.W. Sinton, College of Oceanic and Atmospheric Sciences, Oregon State University, 104 Ocean. Admin. Bldg., Corvallis, OR 97331-5503. (email: csinton@oce.orst.edu)